Role of Grain Boundary Defects During Grain Coarsening of Lamellar Block Copolymers

ARTICLE *in* MACROMOLECULES · DECEMBER 2012

Impact Factor: 5.8 · DOI: 10.1021/ma3015382

Macromolecules

Article

pubs.acs.org/Macromolecules

Role of Grain Boundary Defects During Grain Coarsening of Lamellar Block Copolymers

Hyung Ju Ryu,[†] David B. Fortner,[†] Sukbin Lee,[†,‡] Rachel Ferebee,[†] Marc De Graef,[†] Konstantinos Misichronis,[§] Apostolos Avgeropoulos,[§] and Michael R. Bockstaller[†,*]

[†]Department of Materials Science and Engineering, Carnegie Mellon University, 5000 Forbes Avenue, Pittsburgh, Pennsylvania 15213, United States

[§]Department of Materials Science and Engineering, University of Ioannina, University Campus, Dourouti, 45110, Ioannina, Greece

Supporting Information

ABSTRACT: The evolution of grain size and shape as well as type and frequency of grain boundary structures during thermal annealing of lamellar diblock copolymer microstructures is established using large area image reconstruction and analysis. Grain coarsening is found to proceed via an initial transient stage that is characterized by the rapid relaxation of unstable "frozen-in" defects such as kink boundaries and the subsequent quasi-stationary coarsening that is dominated by the continuous relaxation of low-angle symmetric tilt boundaries. The particular relevance of low-angle symmetric tilt boundaries to grain coarsening is interpreted as the consequence of both the associated decrease of boundary energy as well as the availability of favorable kinetic pathways—such as grain boundary splitting—to facilitate the coarsening process. The inverse relation between grain boundary energy and frequency suggests that the reduction of boundary energy is a relevant governing parameter for the evolution of grain boundary structures—as it is in inorganic materials. The existence of "inert" boundary types (such as asymmetric tilt and twist) that—within the experimental window—do not participate in the coarsening process is expected to have dominant influence on the final morphology that can be attained by thermal annealing of the microstructure. The reduction of the density of inert boundaries during the film preparation process should therefore provide a strategy for increasing the coarsening kinetics in block copolymer films during thermal annealing and thus a path toward a higher degree of order in block copolymer microstructures.

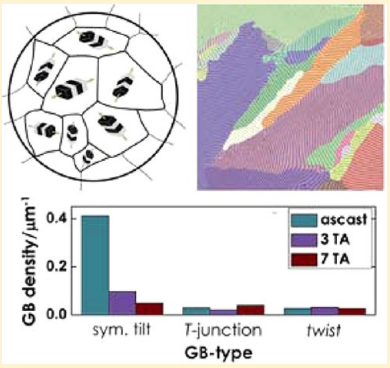

INTRODUCTION

Block copolymers (BCP) are segmented polymers that—owing to their ability to organize into periodic microdomain morphologies—have attracted interest as platform to facilitate technological breakthroughs in areas ranging from optics and sensors to energy generation and storage.[1−9] A common characteristic of many of the proposed applications of BCP-based materials is that the copolymer microstructure serves as a template for functional filler species and that the technology-enabling functionality depends on the transport characteristics of the filler within the matrix. In applications like these, materials performance is expected to strongly depend on the presence of grain boundary (GB) defects because of their impact on both long-range order and tortuosity of diffusion pathways. The basic phenomenology of GB structures in BCP materials was first discussed by Gido and Thomas as well as Hashimoto and co-workers who classified the various GB types associated with tilt and twist deformations of lamellar BCPs.[10−17] Subsequent studies revealed the relevance of process parameters, molecular architecture and composition on GB formation as well as the implications of GB defects on physical properties of BCP materials.[18−22] However, despite of the abundance of GB defects and their demonstrated relevance for material properties, little is known about the governing parameters that control the formation of the various types of GB structures in BCPs nor the evolution of GBs during, for example, the thermal annealing of quiescent organized films (a widely used technique for the preparation of "equilibrated" BCP microstructures). This is in contrast to other classes of materials such as ceramics and metals where it has been widely recognized (and utilized) that the type and frequency of GB structures in materials exert a dominating influence on the evolution of structure and properties during thermal treatment.[23,24] Better understanding of the relevance of GB defects on microstructure evolution in BCP materials, therefore, holds the promise to both novel strategies for the fabrication of BCP microstructures with reduced defect concentrations but also insights into the unifying aspects of defect formation in structured materials.

This article presents a systematic evaluation of the role of GB structures on grain coarsening in lamellar block copolymers during thermal annealing of (quiescent) solution-cast films. Here, the term "grain coarsening" is used to describe the evolution of microstructure in BCP melts in which an initial

Received: July 23, 2012
Revised: October 29, 2012
Published: December 19, 2012

state microstructure has already been developed, for example, by nucleation and growth in solution-cast films. One major result of the present study is that grain growth in lamellar BCPs is associated with the annealing of *particular* types of GB structures (i.e., low-angle symmetric tilt GBs, see discussion below) rather than the uniform reduction of the density of GB defects. The preferential relaxation of low-angle symmetric tilt GBs is interpreted to be a consequence of both the kinetic and thermodynamic parameters that control the annealing of GB structures and is expected to impose constraints to the structural uniformity that can be achieved by thermal annealing of BCP materials.

The organization of this article is as follows: First, a brief summary of previous studies on microstructure formation in BCPs and GB defects will be provided in order to establish the context for the discussion of our results. Subsequently the experimental procedures to analyze structural characteristics such as grain size or type and frequency of GB structures as well as the energy penalty associated with GB formation will be introduced. The evolution of GB structures during thermal annealing of an amorphous lamellar BCP model system will be presented and discussed in terms of the kinetic and thermodynamic parameters that relate to the annealing of the various GB types.

BACKGROUND

Several revealing studies on the ordering kinetics and morphology evolution in BCP materials with lamellar, cylindrical, bicontinuous and spherical morphology have been described during the past 20 years, mostly with focus on grain nucleation and growth. For example, using combined small-angle X-ray scattering and electron microscopy analysis, Hashimoto and co-workers demonstrated the first-order characteristics of the order−disorder transition in BCP materials.[25−27] Using *in situ* depolarized light scattering, Garetz and Balsara demonstrated that under quiescent conditions the formation of ordered microstructures occurs via the initial rapid growth of randomly oriented, ellipsoidal domains that—upon impingement—continue to grow by slow, cooperative effects (defect annihilation stage).[28−34] Chastek and Lodge applied polarized optical microscopy to show that the growth front velocity of forming grains in concentrated BCP solutions is approximately captured by the Goveas−Milner prediction.[35−37]

The formation of ordered domains by nucleation and growth implies the formation of GB defects upon the impingement of adjacent grains at the late stage of the order−disorder phase transformation process. The occurrence of GB defects is therefore inherent in quiescent organized BCP materials and hence films exhibit a granular microstructure constituted of grains with distinct domain orientation separated by homo-phase boundaries (i.e., GB defects). Other possible mechanisms for GB formation have been related to the superposition of stress-fields around disclinations and mechanically induced kinking, for example, induced by inhomogeneous solvent evaporation during the later stages of film formation.[12] The presence of thermodynamically unstable GB defects in the "as-cast" BCP system raises the energy content of the material and provides the energetic driving force for grain growth and microstructural rearrangement during thermal annealing toward a lower energy structural state. This general expectation provides the motivation for the thermal annealing of solution-cast BCP materials as a pathway to realize more uniformly ordered microdomain structures. However, while the principal driving forces for grain growth are well understood, it has been shown for a range of inorganic materials that the mechanism and kinetics of grain growth (and thus the attainable final microstructure) sensitively depend on the characteristics of the GB structures that exist within the material.[23,24] This motivates the systematic evaluation of the relationship between GB characteristics and structure evolution in BCP materials that is the subject of the present contribution.

In general, GB defects in materials with centro-symmetric structure are described in terms of the number of independent parameters (or degrees of freedom) that determine the orientation of the boundary and the adjacent grains. Thus, in the most general case, a GB is described by five macroscopic degrees of freedom that can be associated with the three Euler angles to bring the adjacent lattices into coincidence plus two angles to describe the orientation of the boundary with respect to the grains.[24,38] The different GB arrangements that are associated with the five degrees of freedom are schematically illustrated in Figure 1.

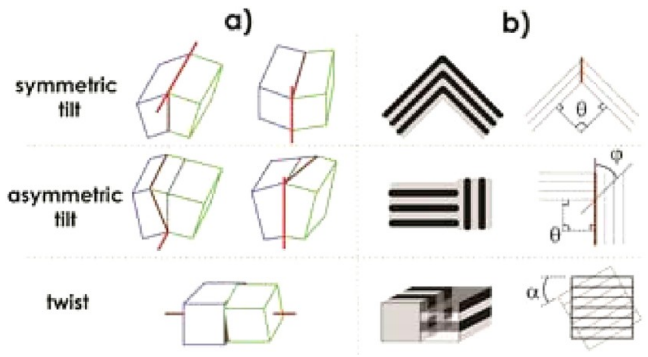

Figure 1. Illustration of possible grain boundary structures in (a) polycrystals and (b) lamellar BCPs. Panel a: Depiction of the five distinguishable deformation modes for a general bicrystal (two symmetric tilt, two asymmetric tilt, one twist). Brown and red lines indicate grain boundaries and rotation axes, respectively. Black dotted lines indicate the symmetry plane between the adjacent grains. Panel b: Illustration of the three fundamental types of grain boundary structures for lamellar structures, where θ, φ, α indicate tilt angle, angle between the boundary plane and the symmetry plane, and twist angle, respectively.

For lamellar microstructures (that are of interest for the present paper) the number of degrees of freedom is reduced to only three due to the symmetry of the structure.[38] Therefore, three fundamental types of GB structures are distinguished in lamellar systems, i.e., symmetric tilt, asymmetric tilt and twist GB structures as indicated in Figure 1.[39] Here, the notion of "tilt" and "twist" refers to the underlying deformation mode of an ideal lamellar bicrystal structure that gives rise to the grain boundary: tilt GBs involve rotation between adjacent grains about an axis in the plane of the boundary while twist GBs involve rotation about an axis normal to the boundary plane. Tilt GBs are further classified as "symmetric" or "asymmetric" depending on whether or not the boundary plane is equal to the mirror plane of the bicrystal (see Figure 1b). Because of the local geometry of material distribution along the respective boundaries, symmetric tilt GBs in lamellar BCP are further differentiated as either chevron (Ch, typically observed at low to intermediate tilt angles) or omega (Ω, typically observed at high tilt angles); asymmetric tilt GBs with 90° tilt angle in which mirror and boundary planes are inclined by 45° are

dx.doi.org/10.1021/ma3015382 | *Macromolecules* 2013, 46, 204−215

denoted *T*-junction GB.[13] It should be noted that the chevron (Ch) and omega (Ω) GB structures represent distinct manifestations of the *same* GB type (i.e., symmetric tilt) and therefore can undergo mutual transformations (see discussion below).

The energy of GB structures is generally expected to be a sensitive function of the orientation between the lattices of the adjacent grains. For crystalline materials the mutual orientation of adjacent crystal grains is often expressed in terms of the "grain misorientation" **g** that describes the distance between the two orientations in orientation space.[24] In case of lamellar structures the misorientation is equal to the angle θ between the lamellar normals of adjacent grains. The orientation of each lamellar normal is determined by two parameters, i.e. the longitude (ϕ_1) and latitude (ϕ_2) that define the orientation of the normal with respect to a reference coordinate system (the latter is chosen to reflect the major directions of the film casting geometry). For the purpose of the following discussion the laboratory reference frame is chosen such that ϕ_1 and ϕ_2 correspond to the in-plane and out-of-plane angle between the normal and the *x*- and *z*-axis of the reference coordinate system as illustrated in Figure 2.

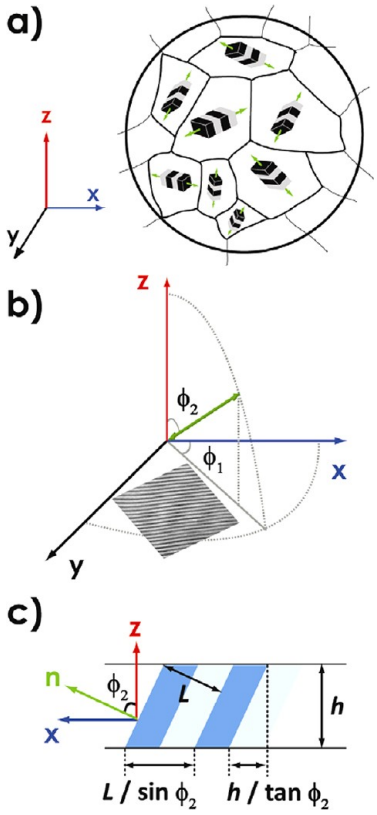

Figure 2. Panel a: Depiction of a typical block copolymer microstructure revealing granular structure. The orientations of lamellae are described with lamellar normals (green arrows) in a given orientation reference frame. The alteration of lamellar normals delimits the boundary network. Panel b: Illustration of the two orientation parameters, longitude (ϕ_1) and latitude (ϕ_2), which define the inclination angles with respect to the *x*- and *z*-axis, respectively. Panel c: Illustration of projection geometry of lamellar film structure. Inclination of lamellar domains results in reduced imaging contrast thus limiting the range of accessible values of latitude values to 65° < ϕ_2 < 115° (see text for more details).

Using the definitions of longitude and latitude, a lamellar normal is then defined as a vector $\mathbf{n} = (n_x, n_y, n_z)$ with $n_x = \cos(\phi_1)\sin(\phi_2)$, $n_y = \sin(\phi_1)\sin(\phi_2)$, and $n_z = \cos(\phi_2)$. Thus, the misorientation θ of two grains (i, j) in a lamellar structure can be represented as a function of the corresponding values of longitude and latitude of the two grains as $\theta = \cos^{-1}(\mathbf{n}_1 \cdot \mathbf{n}_2)$ or equivalently:

$$\theta = \cos^{-1}\left(\frac{n_{x,i}n_{x,j} + n_{y,i}n_{y,j} + n_{z,i}n_{z,j}}{(n_{x,i}^{\,2} + n_{y,i}^{\,2} + n_{z,i}^{\,2})^{1/2}(n_{x,j}^{\,2} + n_{y,j}^{\,2} + n_{z,j}^{\,2})^{1/2}} \right) \quad (1)$$

Note that for symmetric tilt GBs with $\phi_2 = 90°$ the misorientation becomes a function of the longitude only, and thus the misorientation becomes equal to the tilt angle between the adjacent grains.

Groundbreaking work by the Thomas and Hashimoto groups has established the foundation of our current understanding of grain boundary formation in lamellar BCP systems.[11−14,17] For example, Gido and Thomas studied the grain boundary formation in bulk amorphous lamellar BCP materials after long-time annealing and identified various morphologies for twist (helicoid and Scherk surface) and tilt (Ch-, Ω- and *T*-junction) boundaries.[11−14] For symmetric tilt GBs a transition from Ch- to Ω-morphology was observed with increasing angle of tilt; this was rationalized to be a consequence of the packing frustration of chains in the "kink" region of the boundary. Indirect evidence of this thesis has been provided by experimental and theoretical studies of GB formation in BCP/nanoparticle blends that revealed the preferential sequestration of particle fillers within the kink regions of symmetric GBs (that is presumably driven by the associated relaxation of chain conformations in the boundary region).[40,41] Simulation studies by Schick and co-workers as well as Matsen (using a Ginzburg−Landau free energy and self-consistent field approach, respectively) evaluated the GB energy for both symmetric and asymmetric tilt GBs in weakly segregated BCP systems.[42−47] These studies confirmed the observed Ch → Ω transition with increasing misorientation of symmetric tilt GBs and also revealed a significantly higher energy penalty associated with the formation of discontinuous asymmetric tilt GB structures (such as *T*-junction GBs) as compared to their symmetric analogues. Our group recently evaluated the energies of symmetric tilt GB structures in a strongly segregated BCP by triple junction analysis and confirmed the predicted dependence of GB energy on the grain misorientation.[48]

It is important to note that the emphasis of these previous studies was on the characteristics of *individual* GB defects. The present contribution focuses on establishing the relationship between GB type distribution and microstructure evolution in quiescent organized BCPs during thermal annealing. The scope of our work therefore bears similarity to the study of continuous grain growth processes (that occur after recrystallization of inorganic materials such as ceramics and metals) which have been shown to sensitively depend on the details of the respective GB character distribution.[24,49−51] The material system in our study consists of a near-symmetric poly(styrene-*b*-isoprene) (PS−PI) copolymer with molecular weight M_w =

dx.doi.org/10.1021/ma3015382 | *Macromolecules* 2013, 46, 204−215

79.6 kg/mol, a molecular weight dispersity index M_w/M_n = 1.05 and a volume fraction of styrene component of f_{PS} = 0.48. With χ = 0.00785 + 17.6/T for PS−PI the degree of segregation of the BCP at the annealing temperature T = 418 K can be estimated as $\chi N \cong 58$ (where χ denotes the Flory interaction parameter and N the degree of polymerization).[52] Thus, the PS−PI copolymer is in the intermediate to strong segregation regime. Films of 1 mm thickness were cast under rapid solvent evaporation conditions (T = 23 °C, p = 80 mbar) from 5% (w/v) toluene solution to provide for high GB densities during film formation. To determine the evolution of grain size and shape and domain orientation as well as the type and frequency of grain boundary structures during thermal annealing at T = 120 °C, thick films of "as-cast" BCP samples were analyzed using a procedure involving serial electron imaging, image reconstruction, stereology as well as pattern matching and filtering as a function of annealing time (t = 0, 3, and 7 days). The procedure for analyzing the film microstructure is detailed below.

MATERIALS AND METHODS

Materials. Poly(styrene-*b*-isoprene) (PS−PI) copolymer with molecular weight M_w = 79.6 kg/mol, molecular weight dispersity index M_w/M_n = 1.05 and volume fraction of styrene component f_{PS} = 0.48 was synthesized using anionic polymerization as described previously.[53] Styrene, isoprene, and benzene were obtained by Sigma-Aldrich and purified prior to the synthesis by distillation. Toluene was obtained by Sigma-Aldrich and used without purification.

Films of 1 mm thickness were cast from 5% (w/v) toluene solution at T = 23 °C at a pressure of p = 80 mbar (pressure was controlled using a modified Buchi Rotavapor R-200); the time for solvent evaporation was approximately 8 h. Samples were thermally annealed in vacuum at T = 120 °C for 0, 3, and 7 days. Prior to electron imaging films were microsectioned at −120 °C using a LEICA EM FCS cryo-ultramicrotome and stained with OsO_4 (selective staining of PI domains) that was obtained from EM Sciences.

Transmission Electron Microscopy (TEM). Electron imaging of BCP microstructures was performed using a JEOL 2000 EX electron microscope operated at 200 kV. Imaging was based on the amplitude and phase contrast, and images were recorded by a Gatan Orius SC600 high resolution camera.

Microstructure Analysis. At least 50 micrographs at a nominal magnification of 5000× were collected per sample in order to reconstruct sample areas large enough to provide for a statistically relevant analysis of microstructural characteristics.[54−57] Sample sections for microstructure analysis were chosen from the center region of the BCP film in order to avoid artifacts related to the asymmetric interface conditions (i.e., sample/substrate and sample/air). To evaluate the effect of film casting conditions on the BCP microstructure, a (Cartesian) laboratory reference frame was defined such that the film orientation is along the (x, z) plane and the y-direction is normal to the film orientation. For sufficiently thick films substrate interactions can be neglected and therefore the ± directions along the y-axis can be chosen arbitrarily (the absence of polarity was verified for the "as-cast" sample by manual grain analysis, results not shown here). Contiguous areas in excess of 300 μm^2 were reconstructed by manually stitching of electron micrographs. The relationship between sample geometry and laboratory reference frame as well as the procedure of microstructure characterization are illustrated in Figure 3.

As elaborated above, the orientation of lamellae within the microstructure is characterized by two parameters that determine the orientation of the lamellar normal with respect to the reference frame, i.e., the longitude (equal to the in-plane angle between the lamellar normal and x-axis, denoted ϕ_1 in Figures 2b and 3) and the latitude (equal to the out-of-plane angle between the lamellar normal and z-axis, denoted ϕ_2 in Figures 2b and 3). From electron micrographs, the longitude can be directly evaluated from the in-plane orientation of the lamellae whereas the latitude can be determined from the increase of the apparent lamellar repeat distance from its minimum value L (i.e., the lamellar repeat distance corresponding to latitude ϕ_2 = 90°) that is a consequence of the projection of inclined lamellae onto the image plane of the microscope. It is noted that the determination of latitude values based on the analysis of electron micrographs is limited due to ambiguities that arise at larger values of domain inclination depending on lamellar repeat, section thickness and domain contrast. The relation between latitude and lamellar thickness L is illustrated in Figure 2c revealing that the latitude can be determined from the projected lamellar spacing $L' = L/\sin(\phi_2)$. Note that the contrast between adjacent domains vanishes when $h/\tan(\phi_2) = nL(2\sin\phi_2)^{-1}$, or $\phi_2 = \cos^{-1}(nL/2h)$ where h denotes the section thickness and n is an odd integer.[11] The lamellar thickness of the PS−PI was determined to be $L \cong 30$ nm (using small-angle X-ray scattering, results not shown here) and thus the limiting angle can be estimated for a section thickness of h = 60 nm to be $40° < \phi_2 < 140°$. In order to account for variations in the section thickness (based on the interference color of sections the section thickness was estimated to vary during a typical section process between 50 nm < h < 80 nm) for the present system the automated image analysis of grain latitude values could only be considered reliable within the angular range $[65° < \phi_2 < 115°]$. The automated process was therefore complemented by manual analysis of GB structures where appropriate to account for high-angle twist GBs.

To determine longitude and latitude values at each point (i.e., pixel) of large-area electron micrographs, such as the one shown in Figure 3, stitched images were successively processed by thresholding, skeletonization, discretization and Fourier transform analysis (using MATLAB). In a first step, electron micrographs (saved as 8 bit gray

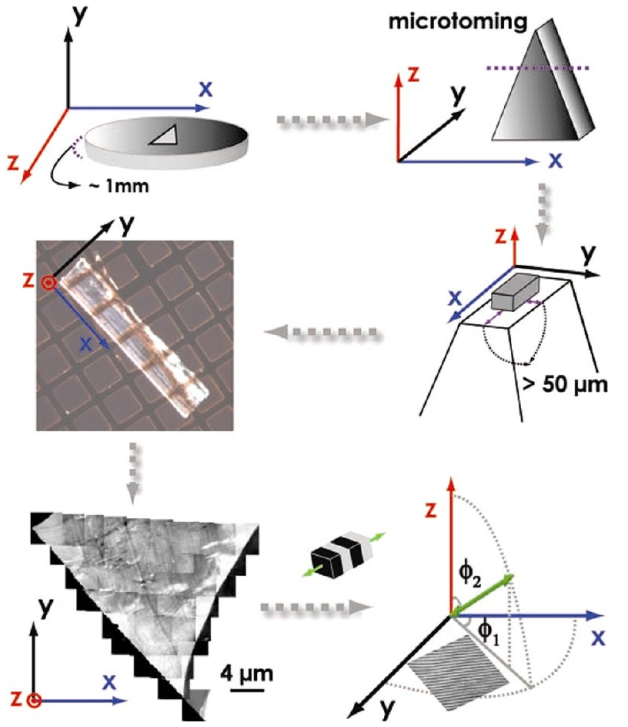

Figure 3. Illustration of the experimental approach employed for the microstructure analysis of lamellar block copolymers. Films of 1 mm thickness are cast by rapid solvent evaporation (see text for more details)—the film casting geometry defines the reference coordinate system for structure analysis (with the x, z-plane denoting the plane of the film substrate). Large contiguous sample areas are reconstructed by serial electron imaging and image analysis. Two orientation parameters, the longitude (ϕ_1, in-plane orientation) and latitude (ϕ_2, out-of-plane orientation) are determined to identify the orientation of grains.

dx.doi.org/10.1021/ma3015382 | *Macromolecules* 2013, 46, 204−215

scale image) were converted to binary image format and subjected to bandpass filtering. This process removes unnecessary information (such as contrast variation resulting from, for example, film thickness variations or knife marks) from the micrographs, but preserves morphological features such as orientation or repeat distance. Images were subsequently skeletonized to convert the binary domain structures into morphologically equivalent line patterns in which lines delineate domain center positions.[58] Discrete Fourier transform analysis was applied to the discretized line patterns (30 × 30 pixel grid size) to determine both the longitude and latitude values at each grid point.

Grain maps were constructed by identification of grid points that separate adjacent areas with a difference in longitude or latitude values in excess of 15°.[59] The application of the image analysis procedure to a representative electron micrograph of "as-cast" PS−PI as well as the resulting grain map is depicted in Figure 4. Note that Figure 4d reveals

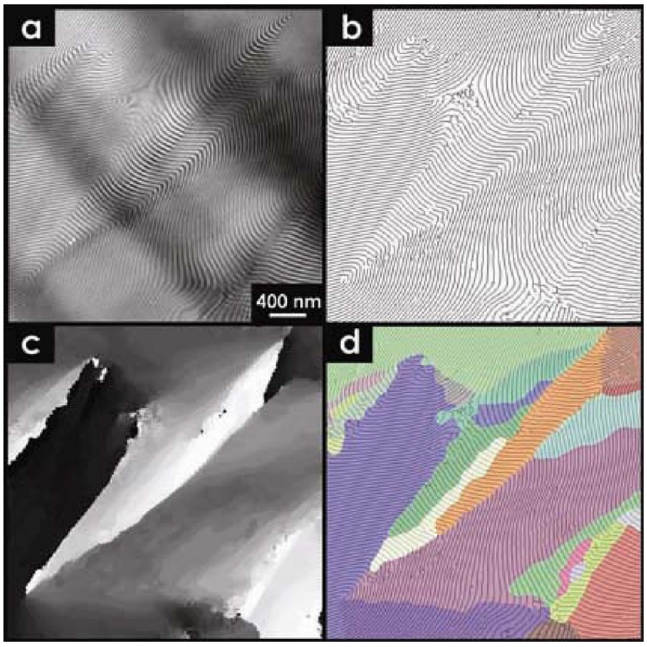

Figure 4. Illustration of representative results of the image analysis procedure described in the text. The original TEM image (panel a) is converted to the skeletonized image (panel b). The lamellar orientation is shown visually as a gray-scaled image in panel c (black and white corresponds to "zero" and 180° longitude value, respectively). Determination of longitude and latitude values yields the grain map shown in panel d, where 15° difference in misorientation was used to identify individual grains.

moderate undulations along low-angle boundaries—these undulations were found to be stable with regard to modifications of the image analysis parameters. It is currently unclear whether these undulations represent artifacts of the image analysis procedure or—as the authors believe—if their origin is of a more fundamental nature (for example, the entropy increase associated with the formation of low-energy distortions of boundaries could provide a driving force for the formation of surface undulations). For the purpose of the present paper the presence of low-angle undulations is of no further consequence.

Provided that the imaged areas allow for adequate sampling of microstructural parameters, the analysis of grain maps (such as Figure 4d) yields important microstructural information such as the distribution of grain size and shape, domain orientation as well as the distribution of type and frequency of GB structures.

A comment should be made regarding potential problems in the interpretation of grain maps such as the one shown in Figure 4 that limit the confidence range for grain sizes to be considered in the subsequent analysis: First, the image thresholding step under realistic conditions necessarily introduces a small (but finite) number of parasitic features with typical length scales approximately equal to the lamellar domain spacing. In the subsequent grain rendering process these features give rise to an artificial increase of the frequency of small grain dimensions. To counter this potential artifact a lower grain size cutoff can be defined such that grains are required to exhibit dimensions greater than two lamellar repeats. A second source of potential artifact formation is the poor statistics associated with grains that exhibit a cross-sectional area comparable to the total reconstructed area. The effect of artifacts due to insufficient statistics can be minimized by restricting the maximum grain size that is considered in the grain size analysis so that sufficient sampling can be expected for all reported grain size dimensions (a practical solution is to limit sampling of grains to areas less than or equal to 10% of the total reconstructed area). In the present study, grain size/shape analysis was therefore limited to grain areas ranging between 0.03−10 μm^2; the reproducibility of results (for example, for the average grain size) from independently analyzed specimens based on this restriction was found to be within 5%.

■ RESULTS AND DISCUSSION

Grain Size and Shape. To elucidate the evolution of microstructural characteristics during thermal annealing, grain maps of PS−PI copolymers were analyzed after 0, 3, and 7 days of thermal annealing (samples are denoted "as-cast", "3 TA" and "7 TA", respectively). Figure 5 depicts representative subsets of grain maps (rotated to render the x-axis horizontally) that were determined from total reconstructed contiguous areas corresponding to 351.9 μm^2 (as-cast), 411.8 μm^2 (3 TA), and 504.8 μm^2 (7 TA).[60]

From Figure 5, the (number) average grain area was determined as 0.9 ± 1.6 μm^2 for as-cast, 1.1 ± 1.7 μm^2 for 3 TA, and 1.6 ± 2.1 μm^2 for 7 TA, respectively, indicating a broad grain size distribution. Figure 6 depicts the respective grain size distributions determined from image analysis (Figure 6a) along with the respective log-normal probability plot (Figures 6b−d). The excellent agreement between the predicted (continuous line) and experimental data in Figures 6b−d confirm that grain size distributions are approximately of log-normal type. It should be noted that the latter presents an analogy to grain size distributions that are frequently encountered in metal or ceramic materials that are subject to normal grain growth.[61] Furthermore, the invariant form of the grain size distribution during annealing suggests that grain coarsening involves the self-similar reorganization of the polymer microstructure (see also discussion of Figure 7 below)—similar to normal grain growth in metals or ceramics.

The region between the arrows in Figure 6b−d is the confidence interval for grain size analysis that forms the basis for the interpretation of grain size and shape during thermal annealing. Figure 7 summarizes the observed trend of grain size and anisotropy during thermal annealing.

Analysis of the data shown in Figure 7 reveals that the average grain size defined as $R(t)$ = (grain area)$^{1/2}$ increases with annealing time following to $R(t) \sim t^{1/n}$ with $n \cong 1.8$ (see dotted line in Figure 7). Because of the limitation of data points it is not possible to derive definitive conclusions about the grain growth mechanism based on the growth exponent; however, it is interesting to note that the exponent is close to values reported for normal grain growth in metal and ceramic structures that typically range from n = 2−4.[61] It has been argued that the growth exponent of a system undergoing normal grain growth reflects the compromise between topological requirements of space-filling of grains and the

dx.doi.org/10.1021/ma3015382 | Macromolecules 2013, 46, 204−215

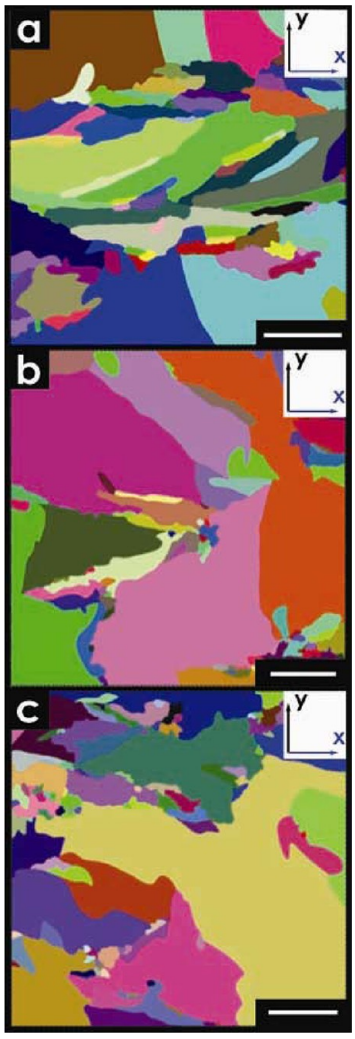

Figure 5. Representative sections of grain maps of PS−PI obtained for as-cast (panel a), 3 days (panel b), and 7 days (panel c) of thermal annealing at T = 120 °C. Image orientation is along x-direction and grains are differentiated by colors. The scale bars are 2 μm. Complete grain maps used for the present study are shown in the Supporting Information.

geometrical constraints associated with boundary surface tension equilibrium.[61,62] The quantitative prediction of the grain growth exponent remains a subject of debate; however, existing theories for grain growth share common features that will briefly be delineated as they have been shown to apply to a wide range of growth processes (and thus are expected to be relevant also for the coarsening of BCP microstructures). A fundamental assumption is that grain growth is driven by the reduction of the total GB energy. Burke and Turnbull were the first to demonstrate that—if topological constraints are neglected—the boundary velocity of growing grains $dR(t)/dt$ is proportional to the driving pressure $P = 2\gamma/\langle R\rangle$ where γ is the GB surface tension and $\langle R\rangle$ is the average grain size. Note that the latter relation implies that the driving pressure for growth decreases with increasing size—this has been interpreted as a prerequisite for self-similar growth. Analysis of the curvature-driven growth model by Burke and Turnbull finds $n = 2$ which typically underestimates experimental values for the growth exponent.[61,62] Various strategies have been pursued to account for the effect of long-range interactions between evolving grains that result from the presence of topological constraints—a common conclusion is that topological constraints will increase n, although a widespread of values has been reported depending on the details of the approach.[63] The expectation of $n > 2$ has been confirmed by a number of recent computer simulations although these studies also point to the relevance of system specific parameters (such as sample geometry, process history or anisotropy of the GB energy) on the grain growth kinetics and a widespread in values of n has been reported.[63,64] It should be mentioned that in the above arguments the GB energy was assumed to be uniform (i.e., all GBs have equal energy). In contrast—as will be shown below—the GB energy in lamellar BCPs is sensitive to the misorientation between adjacent grains. The implications of the GB anisotropy on the growth exponent are currently not clear and a more definitive analysis will require the extension of the current study to a significantly wider range of annealing times.

Interestingly, the stereological analysis of grain maps reveals that grain shapes are anisotropic with an aspect ratio $a/b \cong 2.3$ (where a and b represent the long and short axis of grains, respectively). This is in good agreement with the predicted (and experimentally observed) anisotropy of grains during the nucleation and growth stage of microstructure formation that has been rationalized as a consequence of the anisotropic surface energy of the lamellar structured grains.[25−27,35−37] The decrease of the aspect ratio during thermal annealing indicates that grain growth occurs favorably along the short axis of grains. This confirms previous observations by Dai et al. who used depolarized light scattering to evaluate grain shape evolution during the order−disorder transition of lamellar BCP systems.[28] In the discussion below, the anisotropic growth kinetics will be related to the more rapid annealing of symmetric tilt GB structures that form along the grain long-axis during the solvent casting process.

The evolution of GB-type distributions during thermal annealing is shown in Figure 8. The figure reveals several important characteristics of the grain coarsening process that will be discussed in the following section: First, grain coarsening is predominantly associated with the annealing of symmetric tilt GB structures rather than the uniform reduction of the density of GB defects (see Figure 8a). Second, it is the low-angle range of symmetric tilt GBs that dominate the GB annealing process while higher angle symmetric tilt GBs retain near constant frequency during the annealing process (see Figure 8b). Third, "as-cast" films differ from thermally annealed systems in that a peak in the frequency of high angle symmetric tilt GBs is observed (at a misorientation $\theta \cong 135°$) that rapidly decays during thermal annealing.

We rationalize the particular relevance of symmetric tilt boundaries for the grain coarsening process as a consequence of preferred "GB relaxation pathways" that are not accessible in twist or asymmetric tilt-GB structures. The argument is illustrated in Figure 9, which compares potential GB migration pathways for the case of symmetric and asymmetric tilt GB structures. Provided the absence of external forces to rotate grain orientations, the coarsening process is expected to entail GB migration that in turn depends on both the driving pressure (see discussion above) and the mobility of a boundary that is related to the diffusive processes underlying the motion of GBs. For asymmetric tilt GB structures, two primary migration pathways can be distinguished, *i.e.*, the migration through glide parallel to the boundary or through climb normal to the boundary surface. Both migration processes are considered

dx.doi.org/10.1021/ma3015382 | *Macromolecules* 2013, 46, 204−215

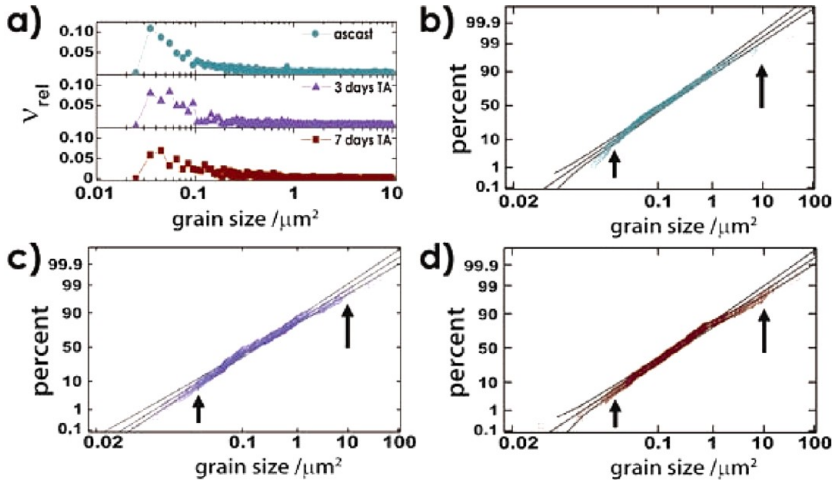

Figure 6. Panel a: Grain size distribution obtained from analysis of grain maps (as shown in Figure 5) within the area range [0.03, 10] μm^2 determined for each thermal annealing time (0, 3, 7 days). Panels b–d: Log-normal probability plots from as-cast (b), 3 days of thermal annealing (c), and 7 days of thermal annealing (d). The middle black line indicates log-normal distribution, and two black lines delineate the 95% confidence interval limits. All grain size distributions are found to approximately follow a log-normal distribution. Arrows in parts b–d indicate confidence range for grain-structure analysis.

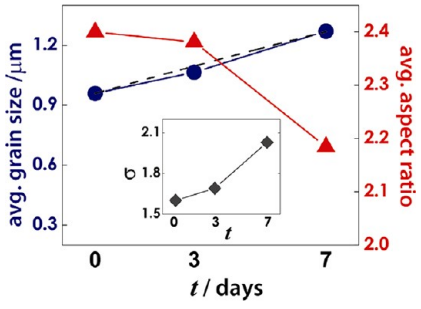

Figure 7. Evolution of average grain size (filled circles) and aspect ratio (filled triangles) of grains during thermal annealing. The average grain size is found to continuously increase during thermal annealing. The dotted line represents the best fit to the data by the Burke and Turnbull model of normal coarsening (see text for more details). Grain aspect ratio is found to decrease during thermal annealing. Shown in the inset is a plot of the standard deviation of grain size σ as a function of thermal annealing time t.

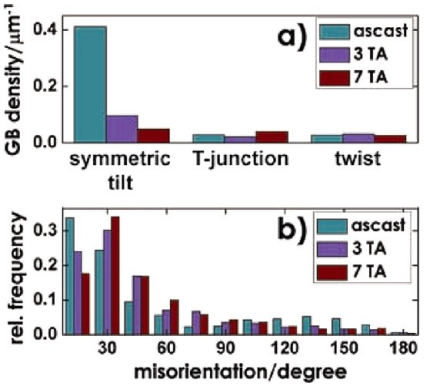

Figure 8. Evolution of grain boundary characteristics during thermal annealing differentiated by grain boundary type (panel a) and angle of misorientation for the particular case of symmetric tilt boundary structures (panel b). Thermal annealing is found to lower the frequency of low-angle symmetric tilt GBs. In as-cast films the frequency of symmetric tilt GBs is peaked at $\theta \cong 135°$, whereas for thermally annealed systems a continuous decrease of the boundary density with increasing tilt angle is observed (see text for more details).

unfavorable since GB climb involves the passage through energetically unfavorable intermediate states and glide is hindered by the geometric constraints of neighboring grains. Thus, asymmetric GB structures are expected to exhibit a reduced mobility and are less likely to contribute to the coarsening process. We note that the manual analysis of the microstructure of the BCP after 28 days of thermal annealing revealed a density of asymmetric tilt and twist GBs of 0.03 and 0.04 μm^{-1}, respectively, thus further confirming the immobile characteristics of these GB types. In contrast, symmetric tilt GBs can contribute to the coarsening process by virtue of an "unzipping" process that involves the transformation of a high-angle symmetric tilt into two (weakly asymmetric) low-angle tilt GBs. Since this process entails shorter diffusive pathways and a more local rearrangement of the copolymer microstructure (in particular the lamellar continuity is preserved during splitting) this GB relaxation pathway should be favorable provided the energy gain associated with the formation of two low-angle boundaries offsets the increase in total boundary area. It should be noted that our study can only provide indirect support of the postulated splitting process of

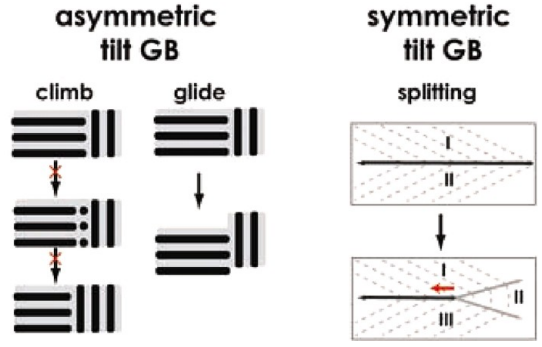

Figure 9. Illustration of possible grain boundary migration pathways for asymmetric and symmetric tilt boundary structures.

symmetric tilt GBs. For example, GB splitting is expected to result in characteristic "Y" arrangements of symmetric tilt GB structures for which ample examples are found in electron

dx.doi.org/10.1021/ma3015382 | Macromolecules 2013, 46, 204–215

micrographs of annealed samples (not shown here). A more definitive proof of the splitting process would entail the direct imaging of symmetric tilt GBs during relaxation—this is a subject of our ongoing research.

The origin of the experimentally observed "inert" character of twist GBs during the coarsening process cannot be resolved with the present study. On the basis of the geometry of the boundary one might expect the migration of a twist boundary (such as a Scherk first surface type, see ref 11) to provide a conceivable path for grain rotation and growth. We hypothesize that the general Arrhenius-type dependence of boundary mobility on the activation barrier of boundary migration could shift the contribution of twist boundaries to the grain coarsening process to longer time scales and thus outside the experimental window of the present study.

Grain Boundary Energy and Annealing. To evaluate the thermodynamic driving force for the proposed splitting of symmetric tilt GB structures, the relative energy of symmetric tilt boundaries was determined as a function of grain misorientation by analysis of the dihedral angles at GB triple junctions. This method is based upon the assumption that the mechanical equilibrium at triple junction lines that are formed by the intersection of three boundaries is determined by the surface tensions of the intersecting boundaries.[65] In this case the angles enclosed between the boundaries at a triple junction (i.e., the dihedral angles) are related to the respective boundary surface tensions via Young's equation: $\sin(\xi_1)/\gamma_1 = \sin(\xi_2)/\gamma_2 = \sin(\xi_3)/\gamma_3$, where ξ_i and γ_i represent the dihedral angle and surface tension of the ith boundary at a given triple junction. Figure 10 illustrates the relevant parameters for the boundary energy analysis.

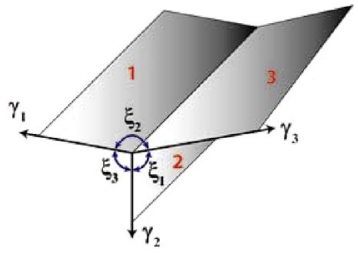

Figure 10. Illustration of grain boundary triple junction geometry and parameters used for grain boundary energy analysis; ξ_i denotes the dihedral angles and γ_i is the surface tension of boundary "i" acting on the triple junction line.

Young's equation yields a set of two independent equations for each triple junction that relate the three unknown boundary tensions to their dihedral angles. By evaluation of a large number of triple junction geometries (here: 1152) a map of the relative GB tensions as a function of tilt angle can be constructed using a statistical procedure that has been detailed in ref 48. Figure 11 depicts the resulting relative surface tension of symmetric tilt GBs for the PS−PI system that was obtained by combining the structural data after 3 and 7 days of thermal annealing. For the reported surface tension analysis of symmetric tilt GBs, boundaries with less than 5° twist contribution and with a disorientation of less than 10° between boundary and symmetry plane were considered as pure symmetric tilt. Data from 3 and 7 days of thermal annealing were combined in order to reduce the error associated with the numerical procedure for evaluating GB surface tensions.[66] The characteristics of $\gamma_{rel}(\theta)$ were discussed in detail in ref 48, and

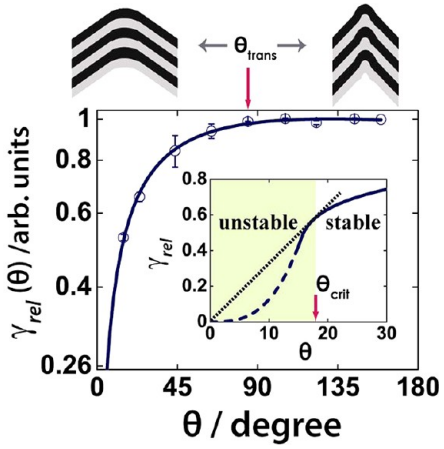

Figure 11. Relative boundary tension map and proposed stability range of symmetric tilt boundary structures (error bars are estimated by the comparison of results after 3 and 7 days of thermal annealing, see text for more details). At the threshold angle $\theta_{trans} \cong 85°$ a transition from the Ch- to the Ω-structure is observed. Inset depicts estimated stability range of symmetric tilt boundaries according to the stability criterion $\gamma_{rel}(\theta) > 2\gamma_{rel}(\theta/2)$ (the dashed line corresponds to theoretical predicted θ^3 dependence at small tilt angles). Spontaneous splitting of symmetric tilt boundaries is expected for $\theta < \theta_{crit} = 18°$.

thus in the following we only highlight the conclusions that are essential with regard to the proposed GB splitting process. In particular, two distinct regimes of the boundary energy can be distinguished in Figure 11 based on their respective dependence on the tilt angle θ. In the limit of small tilt angles ($5° \leq \theta \leq 10°$) the grain boundary energy is found to scale with the tilt angle as $\gamma_{rel}(\theta) \sim \theta^{2.5}$, which is in qualitative agreement with the theoretical predicted scaling $\gamma_{rel}(\theta) \sim \theta^3$ for small tilt deformations of lamellar structures.[42,67] Since the image analysis procedure used in the present study is limited to tilt angles $\theta > 15°$, $\gamma_{rel}(\theta)$ cannot be resolved for angles less than 15°. We hypothesize that the expected scaling θ^3 is present at small tilt angles ($\theta < 15°$) outside the experimental range—this will become an important assumption for the application of $\gamma_{rel}(\theta)$ to interpret the thermodynamic driving force for GB splitting (see discussion below). A plateau regime is observed for angles exceeding $\theta_{trans} \cong 85°$ above which the boundary energy is found to be independent of the tilt angle (within the experimental uncertainty). Electron micrographs reveal that the plateau regime is associated with a transformation of the local structure of symmetric tilt GBs from chevron- to Ω-type as illustrated in Figure 11. This is in agreement with previous studies (both experimental and theoretical) that attributed the Ch → Ω transition of symmetric tilt GBs to the increasingly unfavorable packing situation of chains in Ch boundaries with increasing tilt angle. Within the intermediate tilt angle range, the scaling coefficient of the GB energy relation $\gamma_{rel}(\theta) \sim \theta^x$ is found to continuously decrease with increasing tilt angle within the range $2.5 > x \geq 0$ following to a trend that is in qualitative agreement with previous numerical simulations.[42]

The pronounced change of the scaling coefficient x from the low- to the high tilt angle region reveals a sensitive (and perhaps surprising) angular dependence of the thermodynamic driving force for GB splitting. Assuming that the driving force for GB annealing is dominated by the change in boundary tensions (and thus neglecting the effect of topological constraints), the splitting of symmetric tilt GBs as depicted in Figure 9 will only be energetically favored if the transformation

dx.doi.org/10.1021/ma3015382 | Macromolecules 2013, 46, 204−215

is associated with a decrease of the total GB surface energy. Thus, the condition for GB splitting to be favorable can be approximately stated as $\gamma(\theta) > 2\gamma'(\theta/2)$ where $\gamma(\theta)$ denotes the angle dependent surface tension of the initial symmetric tilt GB prior to the splitting process, and $\gamma'(\theta)$ denotes the tension-relation for the newly formed (weakly asymmetric) low-angle boundaries. If the effect of asymmetry on the grain boundary energy of the newly formed GBs is neglected (i.e., $\gamma(\theta) \cong \gamma'(\theta)$) then the range of tilt angles susceptible to annealing through GB splitting can be estimated from Figure 11 by determination of the tangent to $\gamma_{rel}(\theta)$ that passes through the origin—the abscissa of the tangent identifies the critical misorientation θ_{crit} below which spontaneous splitting is expected.[68] The process is illustrated in the inset of Figure 11 where for illustration purpose the experimental data has been extended to the origin by assuming the predicted θ^3 dependence. Tangent construction reveals that splitting is favorable for $\theta < \theta_{crit} \cong 18°$ and thus only low-angle symmetric tilt GBs are expected to anneal through GB splitting. This conclusion is indeed supported by the experimental data shown in Figure 8 which reveals the frequency of symmetric tilt GBs with $\theta > 30°$ to remain approximately constant after 3 days of thermal annealing. We note that the above estimate for θ_{crit} serves only to semiquantitatively rationalize the observed trend of GB annealing and to illustrate the implications of the specific angle dependence of $\gamma_{rel}(\theta)$. Besides GB tension, other factors such as topological effects and GB−GB interactions could make relevant contributions to the driving potential for grain coarsening and more extensive data sets will be required to draw more affirmative conclusions regarding the relevance of individual contributions to the coarsening process.

Early Stage Coarsening. The analysis of the distribution of tilt GB structures shown in Figure 8b reveals that although the relaxation of low-angle symmetric tilt GBs is common to both 3 and 7 days annealed samples, additional features become apparent for the early annealing stage of "as-cast" films. In particular, Figure 8b reveals that the frequency of symmetric tilt GBs in "as-cast" films is peaked at a tilt angle $\theta \cong 135°$. This is in contrast to annealed systems where the frequency of tilt boundaries continuously decreases with tilt angle (the nature of the "special" high-angle symmetric tilt boundaries in "as-cast" systems will be discussed below). The existence of a particular grain misorientation that rapidly decays during the early coarsening process bears similarity to grain growth processes in metals where grain coarsening commonly involves a transient period of rapid defect relaxation before the microstructure reaches a quasi-stationary state of grain growth.[61] The existence of a "transient" coarsening stage is supported by the analysis of the frequency of symmetric tilt GB structures as a function of GB energy for 0, 3, and 7 days of thermal annealing that is depicted in Figure 12.

Whereas in the case of thermal annealed samples the frequency of GBs is found to continuously decrease with GB energy, the GB frequency in "as-cast" systems—although following the same overall trend—increases in the tail region for high GB energies $\gamma_{rel}(\theta) > 0.95$. We interpret the increase of $\nu(\gamma)$ in the high energy region as a consequence of the increased frequency of GBs at $\theta \cong 135°$ in the "as-cast" system that is illustrated in the inset of Figure 12. Several conclusions can be derived from the data presented in Figure 12. First, the decrease of $\nu(\gamma)$ with increasing γ that is observed in all systems is indicative of the prominent role of boundary energy as a governing parameter for the coarsening of the copolymer

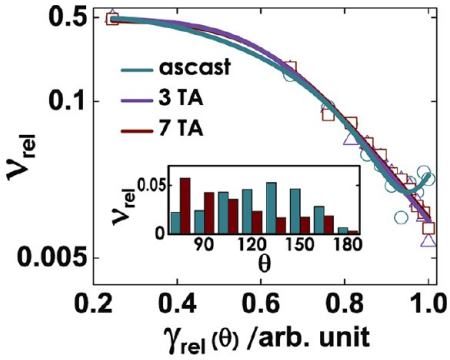

Figure 12. Dependence of the normalized frequency of symmetric tilt GB structures on the boundary energy (determined from data shown in Figures 8 and 11) for 0, 3, and 7 days of thermal annealing. Boundary frequency is found to continuously decrease in case of thermally annealed samples. For as-cast conditions the increase of the boundary frequency is observed at $\gamma_{rel}(\theta) > 0.95$ that is interpreted as a consequence of the high frequency of (unstable) kink boundary structures in "as-cast" films (see text for more details). Inset shows normalized frequency distribution of symmetric high-angle tilt GBs in before (green) and after 7 days (red) of thermal annealing revealing a "peak" of the frequency of high-angle boundaries in "as-cast" condition at $\theta \cong 135°$.

microstructure during thermal annealing (as it is for normal grain growth processes in metals or ceramics).[61] Note that the figure also confirms that GB energy is an influential parameter for structure formation during the solvent-casting process due to the overall similar trend of $\nu(\gamma)$ in case of the "as-cast" BCP system (if the GB energy would not play a role during microstructure formation in "as-cast" systems then a more uniform distribution of $\nu(\gamma)$ would be expected as a result of the random nature of grain impingement). However, the nonmonotonic trend of $\nu(\gamma)$ in the "as-cast" system that is absent from the $\nu(\gamma)$ in annealed BCP films is indicative of an initial transient state of coarsening that we attribute to the relaxation of high-angle tilt GBs (with $\theta \cong 135°$). We attribute the notable role of $\theta \cong 135°$ boundaries during the initial state coarsening of the BCP microstructure to the nonequilibrium character of this boundary type in the "as-cast" state. To substantiate this argument Figure 13 depicts the analysis of high angle symmetric tilt boundaries in "as-cast" films revealing their preferred orientation along the in-plane x-direction of the film (in Figure 13a high-angle symmetric GBs have been highlighted for clarity).

We interpret the increased frequency of high angle tilt GBs in "as-cast" systems to be due to mechanical stresses that act on the microstructure during the late stage of the solvent evaporation process, for example, due to the shrinkage of the film that is constrained by the substrate. These stresses are expected to act predominantly within the plane of the film (similar to biaxial stretch) and could give rise to symmetric high-angle tilt GB structures in stress direction similar to "kink GB" structures that have been observed in lamellar BCP microstructures during deformation.[69−71] We note that the sectioning direction is normal to the observed kink boundaries (see red arrow in Figure 13a) and thus the boundaries cannot be attributed to stresses during the sectioning process. Interestingly, as shown in Figure 13c, the local structure of high-angle symmetric GBs in "as-cast" films is of Ch-type rather than the Ω-type that is observed at identical tilt angles in thermal annealed systems (see Figure 13d). We hypothesize

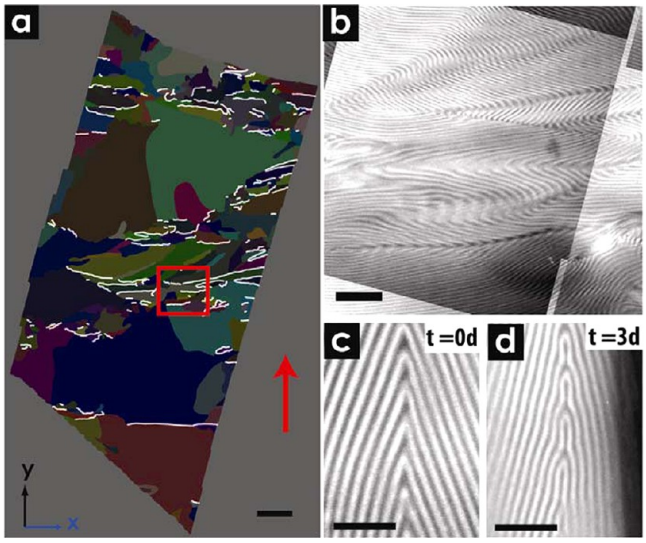

Figure 13. Structure analysis of as-cast PS−PI microstructure revealing formation of kink boundary structures within film plane. Panel a: Grain map of as-cast film with high angle symmetric tilt GBs highlighted as bold white lines. The scale bar corresponds to 2 μm. Orientation of high-angle symmetric tilt boundaries is along in-plane x-direction indicating their origin from stresses within the substrate plane that arise during solvent evaporation (see text for more details). Red arrow indicates sectioning direction. Panel b: TEM image of the area within the red square in part a showing the preferred orientation of kink GBs. The scale bar corresponds to 400 nm. Panel c: TEM image of a typical high angle symmetric tilt boundary ($\theta \cong 140°$) *prior* to thermal annealing revealing Ch-type "kink" structure. Panel d: TEM image of typical high angle symmetric tilt boundary ($\theta \cong 135°$) *after* 3 days of thermal annealing revealing Ω-type structure. The scale bars in parts c and d correspond to 200 nm.

that the unfavorable packing situation that is a characteristic of the high-angle Ch-GBs renders the observed kink structures energetically unstable and thus rapid relaxation of the "frozen-in" kink structures during the initial stage of the coarsening process (presumably through GB splitting) is observed. This assertion is supported by the monotonous decrease of $\nu(\gamma)$ as well as the decrease of the number of "in-plane oriented" kink GBs after 3 days of thermal annealing (not shown here).[72] We note that the relative energy of kink structures cannot be determined using the triple-junction method since the latter is based on the assumption of local equilibrium (which is inconsistent with the notion of "unstable" frozen-in kink structures). However, previous simulation studies (on weakly segregated BCP systems) have indeed revealed a significant energy increase associated with the transformation of Ω- into kink-GB structures in the limit of high tilt angles—it is conceivable that analogous relations will apply to systems in the intermediate and strong segregation regimes.[42] We note that additional evidence for the nonequilibrium character of initial state kink-GBs is provided by the analysis of the local geometry of boundaries. As described above the Ch → Ω transition of symmetric tilt GBs with increasing tilt angle is driven by the increasingly unfavorable packing situation of chains within the kink region of the boundary. Gido and Thomas established the geometric conditions for the Ch → Ω transition using a mean field model and delineated the stability regions of either boundary variant as a function of the boundary geometry.[13] The model predicts that—for a given tilt angle—a Ch → Ω transition is expected when the boundary width W decreases below a critical value that depends on both the tilt angle and BCP characteristics. Figure 14 compares the predicted critical

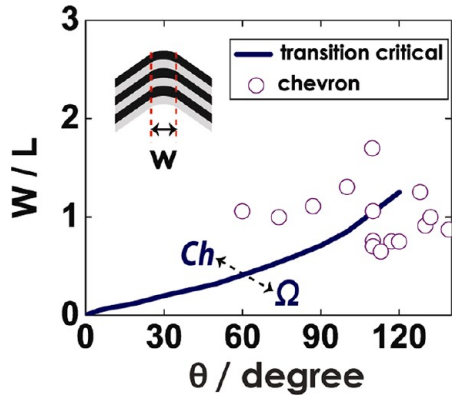

Figure 14. Representation of the normalized width W/L of a representative set of Ch-type boundaries in "as-cast" films (circles) and the calculated critical W/L separating the stability regions for Ch and Ω-type boundaries (solid line, adopted from ref 13). In "as-cast" films the geometrical characteristics of high-angle tilt boundaries (here called kink boundaries) cluster within the Ω-region, thus suggesting the instability of kink boundary structures.

W/L values (blue line) that were adopted from ref 13 for a PS−PI copolymer similar to the present system along with the experimental W/L values for Ch-type boundaries that were obtained using manual analysis from "as-cast" films.

The figure reveals the clustering of high tilt angles Ch-type GBs within the stability region of the Ω−variant thus supporting the unstable character of boundaries of this type (hence the term "kink" boundary is used to differentiate the latter from the stable Ch structure at larger W/L). We note that in thermal annealed films the density of "kink" boundaries was found to be too small to warrant an analysis of the type shown in Figure 14.

CONCLUSIONS

Our results suggest that grain coarsening during the thermal annealing of a solution-cast lamellar model BCP is driven by the energy gain that is associated with the reorganization of GB defects and proceeds by a mechanism that bears similarities to the "continuous grain growth" in metals or ceramic materials. The primary pathway for structural reorganization during annealing is the relaxation of low-angle symmetric tilt GBs. The particular relevance of low-angle symmetric tilt GBs to grain coarsening is interpreted as a consequence of both the associated decrease of boundary energy as well as the availability of favorable kinetic pathways—such as GB splitting—to facilitate the coarsening process. In contrast, the characteristic density of asymmetric tilt and twist boundaries is (within the experimental time frame) unchanged during annealing—a finding that we interpret as evidence for the lower mobility of these types of GB structures. In addition to the annealing of low-angle symmetric tilt boundaries, the early state annealing process is found to entail the relaxation of "frozen-in" kink boundary defects (that we interpret to be a consequence of mechanical stresses that arise during film preparation). We therefore propose that the BCP coarsening process involves two subsequent stages—an initial transient period that is characterized by the rapid relaxation of unstable "frozen-in" high-energy defects such as kink boundaries and the

dx.doi.org/10.1021/ma3015382 | *Macromolecules* 2013, 46, 204−215

subsequent quasi-stationary coarsening by continuous relaxation of symmetric tilt boundaries. We note that the extent to which initial stage coarsening affects the annealing behavior of a BCP will sensitively depend on the process history of the system and the associated density of unstable defect configurations.

The observation of GB structures that do not participate in the annealing process (such as asymmetric tilt and twist boundaries) is an important aspect of the present study. This is because "inert" boundaries are expected to impose constraints on the structural uniformity that can be achieved by thermal annealing of quiescent organized BCP materials. For example, recent theoretical studies on the structure evolution in metals have established a direct link between the final grain size achievable by thermal annealing and the topological constraints that are associated with immobile boundary defects.[73] The control of the density of inert boundaries during the film casting process should therefore be an important prerequisite to facilitate BCP microstructures that are capable of more rapid coarsening and thus of forming "more ideal" microstructures. Drawing on the established understanding of the effect of alloying elements on structure evolution in metals, one strategy for modulating GB formation in BCPs should be the addition of fillers that are capable of selective interactions with GB defects. This motivates the analysis of the effect of (homopolymer) additives on the coarsening characteristics of BCP blend materials that will be the subject of a forthcoming publication.

■ ASSOCIATED CONTENT

Supporting Information

Full grain maps used for analysis of film microstructure. This material is available free of charge at www.acs.org.This material is available free of charge via the Internet at http://pubs.acs.org.

■ AUTHOR INFORMATION

Corresponding Author

*E-mail: bockstaller@cmu.edu.

Present Address

‡School of Mechanical and Advanced Materials, Ulsan National Institute of Science and Technology (UNIST), 100 Banyeon-ri, Eonyang-eup, Ulju-gun, South Korea.

Notes

The authors declare no competing financial interest.

■ ACKNOWLEDGMENTS

This work was primarily supported by the National Science Foundation via grants DMR-0706265, DMR-1006473, EEC-0836633 as well as DMR-0804770. H.J.R. acknowledges Bertucci Graduate Fellowship support. Furthermore, the authors thank the members of the Mesoscale Interphase Mapping Project (MIMP) at Carnegie Mellon for helpful discussions as well as one of the reviewers for pointing out prior work of John W. Cahn regarding the number of independent parameters of grain boundary interfaces.

■ REFERENCES

(1) Park, C.; Yoon, J.; Thomas, E. L. *Polymer* **2003**, *44*, 6725.

(2) Bockstaller, M. R.; Mickiewicz, R. A.; Thomas, E. L. *Adv. Mater.* **2005**, *17*, 1331.

(3) Warren, S. C.; Messina, L. C.; Slaughter, L. S.; Kamperman, M.; Zhou, Q.; Gruner, S. M.; DiSalvo, F. J.; Wiesner, U. *Science* **2008**, *320*, 1748.

(4) Fink, Y.; Urbas, A. M.; Bawendi, M. G.; Joannopoulos, J. D.; Thomas, E. L. *J. Lightwave Technol.* **1999**, *17*, 1963.

(5) Bockstaller, M. R.; Thomas, E. L. *J. Phys. Chem. B* **2003**, *107*, 10017.

(6) Bockstaller, M. R.; Thomas, E. L. *Phys. Rev. Lett.* **2004**, *93*, 166106.

(7) Bockstaller, M. R.; Kolb, R.; Thomas, E. L. *Adv. Mater.* **2001**, *13*, 1783.

(8) Kang, Y.; Walish, J. J.; Gorishnyy, T.; Thomas, E. L. *Nat. Mater.* **2007**, *6*, 957.

(9) Crossland, E. J. W.; Kamperman, M.; Nedelcu, M.; Ducatl, C.; Wiesner, U.; Smilgier, D.-M.; Toombes, G. E. S.; Hillmyer, M. A.; Ludwigs, S.; Steiner, U.; Snaith, H. J. *Nano Lett.* **2009**, *9*, 2807.

(10) Listak, J.; Jakubowski, W.; Mueller, L.; Plichta, A.; Matyjaszewski, K.; Bockstaller, M. R. *Macromolecules* **2008**, *41*, 5919−5927.

(11) Gido, S. P.; Gunther, J.; Thomas, E. L.; Hoffman, D. *Macromolecules* **1993**, *26*, 4506.

(12) Gido, S. P.; Thomas, E. L. *Macromolecules* **1994**, *27*, 849.

(13) Gido, S. P.; Thomas, E. L. *Macromolecules* **1994**, *27*, 6137.

(14) Gido, S. P.; Thomas, E. L. *Macromolecules* **1997**, *30*, 3739.

(15) Gido, S. P.; Schwark, D. W.; Thomas, E. L.; Goncalves, M. D. C. *Macromolecules* **1993**, *26*, 2636.

(16) Burgaz, E.; Gido, S. P. *Macromolecules* **2000**, *33*, 8739.

(17) Nishikawa, Y.; Kawada, H.; Hasegawa, H.; Hashimoto, T. *Acta Polym.* **1993**, *44*, 247.

(18) Kinning, D. J.; Thomas, E. L.; Ottino, J. M. *Macromolecules* **1987**, *20*, 1129.

(19) Csernica, J.; Baddour, R. F.; Cohen, R. E. *Macromolecules* **1987**, *20*, 2468.

(20) Csernica, J.; Baddour, R. F.; Cohen, R. E. *Macromolecules* **1989**, *22*, 1493.

(21) Premnath, V. *J. Membr. Sci.* **1996**, *110*, 133.

(22) Cohen, Y.; Thomas, E. L. *Macromolecules* **2003**, *36*, 5265.

(23) Holm, E. A.; Miodownik, M. A.; Rollett, A. D. *Acta Mater.* **2003**, *51*, 2701.

(24) Rohrer, G. S. *Annu. Rev. Mater. Res.* **2005**, *35*, 99.

(25) Hashimoto, T.; Sakamoto, N.; Koga, T. *Phys. Rev. E* **1996**, *54*, 5832.

(26) Sakamoto, N.; Hashimoto, T. *Macromolecules* **1998**, *31*, 3292.

(27) Sakamoto, N.; Hashimoto, T. *Macromolecules* **1998**, *31*, 3815.

(28) Dai, H. J.; Balsara, N. P.; Garetz, B. A.; Newstein, M. C. *Phys. Rev. Lett.* **1996**, *77*, 3677.

(29) Garetz, B. A.; Balsara, N. P.; Dai, H. J.; Wang, Z.; Newstein, M. C.; Majumdar, B. *Macromolecules* **1996**, *29*, 4675.

(30) Newstein, M. C.; Garetz, B. A.; Balsara, N. P.; Change, M. Y.; Dai, H. J. *Macromolecules* **1998**, *31*, 64.

(31) Kim, W. G.; Chang, M. Y.; Garetz, B. A.; Newstein, M. C.; Balsara, N. P.; Lee, J. H.; Hahn., H.; Patel, S. S. *J. Chem. Phys.* **2001**, *114*, 10196.

(32) Kim, W. G.; Garetz, B. A.; Newstein, M. C.; Balsara, N. P. *J. Polym. Sci. B: Poly. Phys* **2001**, *39*, 2231.

(33) Chang, M. Y.; Abuzaina, F. M.; Kim, W. G.; Gupton, J. P.; Garetz, B. A.; Newstein, M. C.; Balsara, N. P.; Yang, L.; Gido, S. P.; Cohen, R. E.; Boontongkong, Y.; Bellare, A. *Macromolecules* **2002**, *35*, 4437.

(34) Balsara, N. P.; Marques, C. M.; Garetz, B. A.; Newstein, M. C.; Gido, S. P. *Phys. Rev. E* **2002**, *66*, 052802.

(35) Chastek, T. Q.; Lodge, T. P. *Macromolecules* **2004**, *37*, 4891.

(36) Chastek, T. Q.; Lodge, T. P. *J. Polym. Sci. B: Poly. Phys* **2005**, *43*, 405.

(37) Chastek, T. Q.; Lodge, T. P. *J. Polym. Sci. B: Poly. Phys* **2005**, *44*, 481.

(38) The three degrees of freedom in lamellar microstructures can be rationalized by the following procedure: the total number of parameters needed to describe the structure of the interface is six (since two angles are needed to specify the orientation of each lamellar grain as well as the GB interface). Since (in the absence of an aligning field) the properties of the interface are invariant with respect to an

arbitrary rigid body rotation of the entire system, the number of independent degrees of freedom is DOF = 6 − 3 = 3. The same rationale can be applied to arbitrary 3D crystal structures to yield DOF = 8 − 3 = 5 (Cahn, J. W. Unpublished results). We note that other thermodynamic variables (such as temperature and pressure) add to the total number of degrees of freedom. Thus in the most general case there are seven degrees of freedom associated with GB defects. Since (p, T) are generally constant during microstructure evolution only the five "structural" degrees of freedom are typically associated with GBs.

(39) Note that besides these fundamental types of GB structures any mixed type is possible in real microstructures.

(40) Listak, J.; Bockstaller, M. R. *Macromolecules* **2006**, *39*, 5820.

(41) Thompson, R. B. *J. Chem. Phys.* **2010**, *133*, 144902.

(42) Matsen, M. W. *J. Chem. Phys.* **1997**, *107*, 8110.

(43) Netz, R. R.; Andelman, D.; Schick, M. *Phys. Rev. Lett.* **1997**, *79*, 1058.

(44) Villain-Guillot, S.; Netz, R. R.; Andelman, D.; Schick, M. *Physica A* **1998**, *249*, 285.

(45) Tsori, Y.; Andelman, D.; Schick, M. *Phys. Rev. E* **2000**, *61*, 2848.

(46) Duque, D.; Katsov, K.; Schick, M. *J. Chem. Phys.* **2002**, *117*, 10315.

(47) Duque, D.; Schick, M. *J. Chem. Phys.* **2000**, *113*, 5525.

(48) Ryu, H. J.; Fortner, D. B.; Rohrer, G. S.; Bockstaller, M. R. *Phys. Rev. Lett.* **2012**, *108*, 107801.

(49) We note that besides GB structures the annealing of one-dimensional defects makes a contribution to the coarsening process. For a more detailed discussion of the role of dislocations on microstructure evolution in cylindrical and spherical BCP microstructures the reader is referred to references 50 and 51.

(50) Harrison, C.; Adamson, D. H.; Cheng, Z.; Sebastian, J. M.; Sethuraman, S.; Huse, D. A.; Register, R. A.; Chaikin, P. M. *Science* **2000**, *290*, 1558.

(51) Segalman, R. A.; Hexemer, A.; Hayward, R. C.; Kramer, E. J. *Macromolecules* **2003**, *36*, 3272.

(52) Balsara, N. P. Thermodynamics of Polymer Blends. In *Physical Properties of Polymer Handbook*; Mark, J. E., Ed.; AIP: New York, 1996.

(53) Listak, J.; Hakem, I. F.; Ryu, H. J.; Rangou, S.; Politakos, N.; Misichronis, K.; Avgeropoulos, A.; Bockstaller, M. R. *Macromolecules* **2009**, *42*, 5766.

(54) It should be noted that alternative techniques for the direct 3D reconstruction of BCP microstructures such as confocal microscopy (CM) or electron tomography (ETOM) were evaluated but found to be not suitable. Specific limitations entail the need of high molecular weights to resolve the BCP microdomain structure (CM) that implies a dramatic slowdown of ordering kinetics and the limitation to section thicknesses less than the average grain size (ETOM)—for more information the reader is referred to references 55−57. New opportunities for the direct reconstruction of large volumes are provided by emerging X-ray tomographic techniques. The application of these techniques to the characterization of BCP microstructures is the subject of our ongoing research.

(55) Jinnai, H.; Sawa, K.; Nishi, T. *Macromolecules* **2006**, *39*, 5815.

(56) Jinnai, H.; Spontak, R. J.; Nishi, T. *Macromolecules* **2010**, *43* (4), 1675.

(57) Lee, W.; Yoon, J.; Lee, H.; Thomas, E. L. *Macromolecules* **2007**, *40*, 6021.

(58) Pratt, W. K. *Digital Image Processing*, 4th ed.; Wiley-Interscience: NJ, 2007.

(59) A threshold angle of 15° was determined such as to balance reliable grain identification as well as the required computation time for image processing.

(60) For the depiction of full grain maps the reader is referred to the Supporting Information.

(61) Humphreys, F. J. and Hatherly, M. *Recrystallization and Related Annealing Phenomena*, 2nd ed.; Elsevier: Oxford, U.K., 2004.

(62) Burke, J.; Turnbull, D. *Prog. Met. Phys.* **1952**, *3*, 220.

(63) Mullins, W. W. *Acta Mater.* **1998**, *46*, 6219.

(64) Frary, M.; Schuh, C. A. *Acta Mater.* **2005**, *53*, 4323.

(65) Mechanical equilibrium implies the intersection of exactly three boundaries, higher order intersection lines are expected to dissociate into sets of triple junctions.

(66) Since local thermal equilibrium at triple junctions should be established after short annealing times, both annealing conditions are expected to yield identical results. This was confirmed by comparison of the results of the individual analysis of GBs formed after 3 and 7 days, however, because of the larger error margin the result for the combined data set is presented here.

(67) De Gennes, P. G.; Prost, J. *The Physics of Liquid Crystals*: Oxford University Press: Oxford, U.K., 1993.

(68) The representation of the low-angle GBs formed during the splitting process as "symmetric" is only an approximation since the generated GBs are necessarily asymmetric (and thus $\gamma(\theta)$ and $\gamma'(\theta)$ are not identical)—the error associated with this approximation decreases with decreasing tilt angle. Since the present discussion focuses on low-angle boundaries the approximation $\gamma(\theta) \cong \gamma'(\theta)$ is expected to be valid.

(69) Read, D. J.; Duckett, R. A.; Sweeney, J.; McLeish, T. C. B. *J. Phys. D: Appl. Phys.* **1999**, *32*, 2087.

(70) Winey, K. I.; Qiao, L. *Macromolecules* **2000**, *33*, 851.

(71) Laurer, J. H.; Pinheiro, B. S.; Polis, D. L.; Winey, K. I. *Macromolecules* **1999**, *32*, 4999.

(72) An alternative route towards the relaxation of stresses would be the Ch → Ω transformation of kink structures. The decrease of the frequency of in-plane oriented high-angle tilt GBs suggests that GB splitting is the preferred relaxation pathway.

(73) Holm, E. A.; Foiles, S. M. *Science* **2010**, *328*, 1138.